Estimation of Canopy Height From a Multi-SINC Model in Mediterranean Forest With Single-Baseline TanDEM-X InSAR Data

Tao Zhang, Haiqiang Fu, *Senior Member, IEEE*, Jianjun Zhu, Juan M. Lopez-Sanchez, *Senior Member, IEEE*, Cristina Gómez, Changcheng Wang, *Member, IEEE*, Wenjie He, and Zhiwei Liu

***Abstract*—TanDEM-X interferometric synthetic aperture radar (InSAR) data have demonstrated promising advantages and potential in recent years for the inversion of forest height. InSAR coherence becomes the primary input feature when a precise digital terrain model is unavailable, but the relationship between InSAR coherence and forest height remains uncertain because of the complexity of forest scenes. In this article, a method for retrieving canopy height in Mediterranean forests, characterized by short and sparse trees, using a single-pass bistatic TanDEM-X InSAR dataset is proposed. To improve the accuracy of forest height inversion from the uncertain correlation between InSAR coherence and canopy height, we begin by using the established SINC model with two semiempirical parameters and then expand the single curve into a collection of three curves, forming the multi-SINC model. To determine the optimal relationship (curve) between TanDEM-X InSAR coherence and canopy height, the problem is shifted from parameter inversion to classification. To solve the problem, we used optical remote sensing data, a small amount of light detection and ranging (LiDAR) data, and TanDEM-X InSAR data in combination with machine learning for classification. As a proof-of-concept, we conducted forest height retrieval at two study sites in Spain with complex terrain and diverse forest types. The results were verified by comparing them with LiDAR product forest height, which demonstrated improved performance (RMSE = 2.49 m and 1.7 m) compared with the semiempirical SINC model (RMSE = 3.28 m and 2.36 m).**

***Index Terms*—Coherence, forest height, interferometric synthetic aperture radar (InSAR), machine learning (ML), multi-SINC, TanDEM-X.**

Manuscript received 17 September 2023; revised 28 December 2023 and 18 January 2024; accepted 28 January 2024. Date of publication 7 February 2024; date of current version 4 March 2024. This work was supported in part by the National Key Research and Development Program of China under Grant 2022YFB3902605, in part by the National Natural Science Foundation of China under Grant 42227801, in part by the Natural Science Foundation for Excellent Young Scholars of Hunan Province under Grant 2023JJ20061, in part by the Spanish Ministry of Science and Innovation (State Agency of Research, AEI), and in part by the European Funds for Regional Development under Project PID2020-117303GB-C22/AEI/10.13039/501100011033. *(Corresponding author: Haiqiang Fu.)*

Tao Zhang, Haiqiang Fu, Jianjun Zhu, Changcheng Wang, and Wenjie He are with the School of Geosciences and Info-Physics, Central South University, Changsha 410083, China (e-mail: truechang@csu.edu.cn; haiqiangfu@csu.edu.cn; zjj@csu.edu.cn; wangchangcheng@csu.edu.cn; hewenjie@csu.edu.cn).

Juan M. Lopez-Sanchez is with the Instituto Universitario de Investigación Informática, University of Alicante, 03080 Alicante, Spain (e-mail: juanmalopez@ieee.org).

Cristina Gómez is with the iuFOR-EiFAB Campus de Soria, University of Valladolid, 42004 Soria, Spain, and also with the University of Aberdeen, AB243UE Aberdeen, U.K. (e-mail: cgomez@uva.es).

Zhiwei Liu is with the School of Geosciences and Info-Physics, Central South University, Changsha 410083, China, and also with the University Institute for Computer Research, University of Alicante, 03080 Alicante, Spain (e-mail: liuzhiwei@csu.edu.cn).

Digital Object Identifier 10.1109/JSTARS.2024.3363051

I. Introduction

ACHIEVING forest height mapping with high accuracy and high spatial resolution is crucial since the forested areas cover more than 30% of Earth's land [1]. Moreover, forest height is considered a key input variable in the estimation of aboveground biomass, which is essential for understanding the global carbon cycle [2], [3]. Remote sensing techniques provide the possibility to extract forest parameters on a large scale. Optical remote sensing provides the surface information about forests, but it may be hindered by cloud cover and has limited capability to measure canopy height. Airborne light detection and ranging (LiDAR) is commonly used as validation data since it is capable of accurately measuring forest height, but it lacks the ability of large-scale mapping. Spaceborne LiDAR, such as ICESat-2 [4] and GEDI [5], collects discrete point data to determine forest height, which is commonly used as control points in wall-to-wall forest height measurements [6]. Interferometric synthetic aperture radar (InSAR) has been regarded as a potential tool for estimating forest height due to its strong penetrability and high sensitivity to the physical characteristics of forests [7], [8], [9].

It is difficult to obtain the observations required for inverting canopy height from existing repeat-pass InSAR systems due to temporal decorrelation and inappropriate interferometric baseline lengths [10], [11], [12], [13]. TerraSAR-X and TanDEM-X, launched by the German Space Agency (DLR) in 2007 and 2010, respectively, constitute a bistatic interferometric configuration with the objective of generating a global digital elevation model (DEM) of high resolution and precision [13], [14], [15], [16], [17]. In such a case, interferometric observations are unaffected by the temporal decorrelation and atmospheric delay, so they can be used to estimate forest height by exploiting physical models or empirical relationships [13], [18], [19], [20].

A physical model is commonly employed to define the relationship between InSAR observations and forest height [4], [8], [21], [22], [23]. Forest height can be retrieved through the

analysis of TanDEM-X InSAR backscattering data or employing mathematical statistics' techniques [24], [25], [26], [27]. Beyond that, the random volume over ground (RVoG) model is widely used for retrieving forest height from InSAR data [7], [8]. To make the model solvable, fully polarimetric or multiple-baseline data are required to estimate all the model parameters, i.e., forest height, ground phase, extinction coefficient, and ground-to-volume amplitude ratio [6].

However, an imbalance appears when the RvoG model is applied to invert forest height with conventional single-polarization single-baseline TanDEM-X InSAR data since the four unknowns (model parameters) cannot be solved with just two observations (interferometric phase and coherence) [18], [28], [29], [30]. One of the effective schemes to solve the issue of insufficient observations is using external data such as a precise DTM for the ground topography [21]. However, the accurate DTM covering wide areas is usually unavailable for forested regions [21], [31], [32]. Another strategy consists in simplifying the RvoG model by applying diverse assumptions. For example, the SINC function model and its improved versions have been proposed [29], [30], in which the InSAR coherence magnitude is directly related to the canopy height [12]. However, the model simplification process can introduce new errors, mainly reflecting that it cannot accurately describe the actual correspondence between forest height and InSAR coherence for different datasets. For instance, TanDEM-X InSAR data are characterized by different baselines that exhibit varying sensitivity to the forest height [23], [33]. With such a diverse sensitivity, the observed coherence for the same forested area may differ greatly from one dataset to another. To settle this mismatch between InSAR sensitivity to height and specific forest properties, which also depend on the scene, the semiempirical SINC (SeEm-SINC) model was proposed [29], [30], [34], [35].

Unfortunately, the relationship between TanDEM-X InSAR coherence and forest height is not one-to-one due to the complexity of forested areas, and one value of coherence may be caused by trees with different heights even when only one certain interferometric pair is processed. Therefore, matching adaptive semiempirical parameters for each pixel in the interferogram is a challenging task because adequate prior information should be provided. Our objective in this work is to propose an effective approach for improving the performance of the SeEm-SINC. Since the correspondence between different TanDEM-X InSAR coherence and forest heights needs to be reconsidered, this relationship should be refined to be adaptive in complex scenes, especially in the presence of short and sparse forests. With this purpose, the single curve in the existing SeEm-SINC model is expanded into multiple curves to further optimize the corresponding relationship between InSAR coherence and forest height. This yields a new methodology referred to here as the multi-SINC model. The problem of parameter inversion is transformed into a classification problem in which there are several sets of semiempirical parameters available for each pixel.

Our objective is to utilize machine learning (ML) to identify the optimal class of semiempirical parameters and thereby establish a comprehensive method for inverting forest height over complicated forested areas using single-pass bistatic TanDEM-X InSAR data. To support this approach, we leverage a subset of LiDAR products that capture forest height, along with optical remote sensing data. By estimating forest height with multi-SINC model, this article proposed an enhanced method to improve the accuracy.

TABLE I
INFORMATION ON TANDEM-X INSAR DATA EMPLOYED AT THE TWO STUDY SITES

Study site	Date	HoA	Orbit	θ	Resolution (Range * Azimuth)
La Rioja	12/28/2012	34.76 m	Asc.	34.75°	3.09 * 3.30 m
Teruel	10/23/2012	31.67 m	Asc.	37.10°	2.93 * 3.30 m

The rest of this article is organized as follows. Section II introduces two study sites with complexity in Spain. It summarizes experimental data, including TanDEM-X InSAR data for forest height inversion and LiDAR production for validation, as well as optical remote sensing data for assistance. Section III provides detailed explanations of the semiempirical model based on the SINC function and multi-SINC model, along with the calculation method for forest height. The results are presented in Section IV. The discussion is derived from the study, followed by an analysis of the potential for future forest height mapping in Section V. Finally, Section VI concludes this article.

II. STUDY SITE AND DATASETS

A. Study Sites

Two study sites located in Spain are chosen to validate the proposed method: La Rioja and Teruel [see Fig. 1(a)]. The selected study sites are representative of the complex scenarios of Mediterranean forests, characterized by a large diversity of forest species. To be well managed, the existing forest types and species have been reclassified into six classes: Conifer 1, Conifer 2, Broad 1, Broad 2, Mixed 1, and Mixed 2. In addition to the diverse forest species, the study sites are characterized by complex terrain with numerous mountainous regions and a topographical variation spanning 1500 m. Another notable feature is that the forest is shorter than tropical or subtropical forests, with the mean canopy height of the two study sites being approximately 12 m, with a maximum height of about 30 m and mainly concentrated at 5–20 m. Overall, by setting the Spanish forest map as the reference data, the forest coverage is 51.85% and 69.95% at the two study sites.

B. TanDEM-X InSAR Data

The information of the two TanDEM-X coregistered single-look slant-range complex (CoSSC) radar products employed in this work is listed in Table I. The height of ambiguity (HoA) of the two InSAR pairs is 34.76 and 31.46 m, which is appropriate for short forest height estimation according to the previous research [23], [33]. At the two study sites, the TanDEM-X acquisitions were obtained from ascending single-polarization (HH) InSAR data. The resolution of the CoSSC data is approximately 3 m in ground range and 3.30 m in azimuth. When we processed with the original SLC data, the coherence is estimated directly, followed by a 4×4 multilooking process with the GAMMA software, resulting in products with a spatial resolution of approximately 12 m. To attain high-resolution products, it is crucial

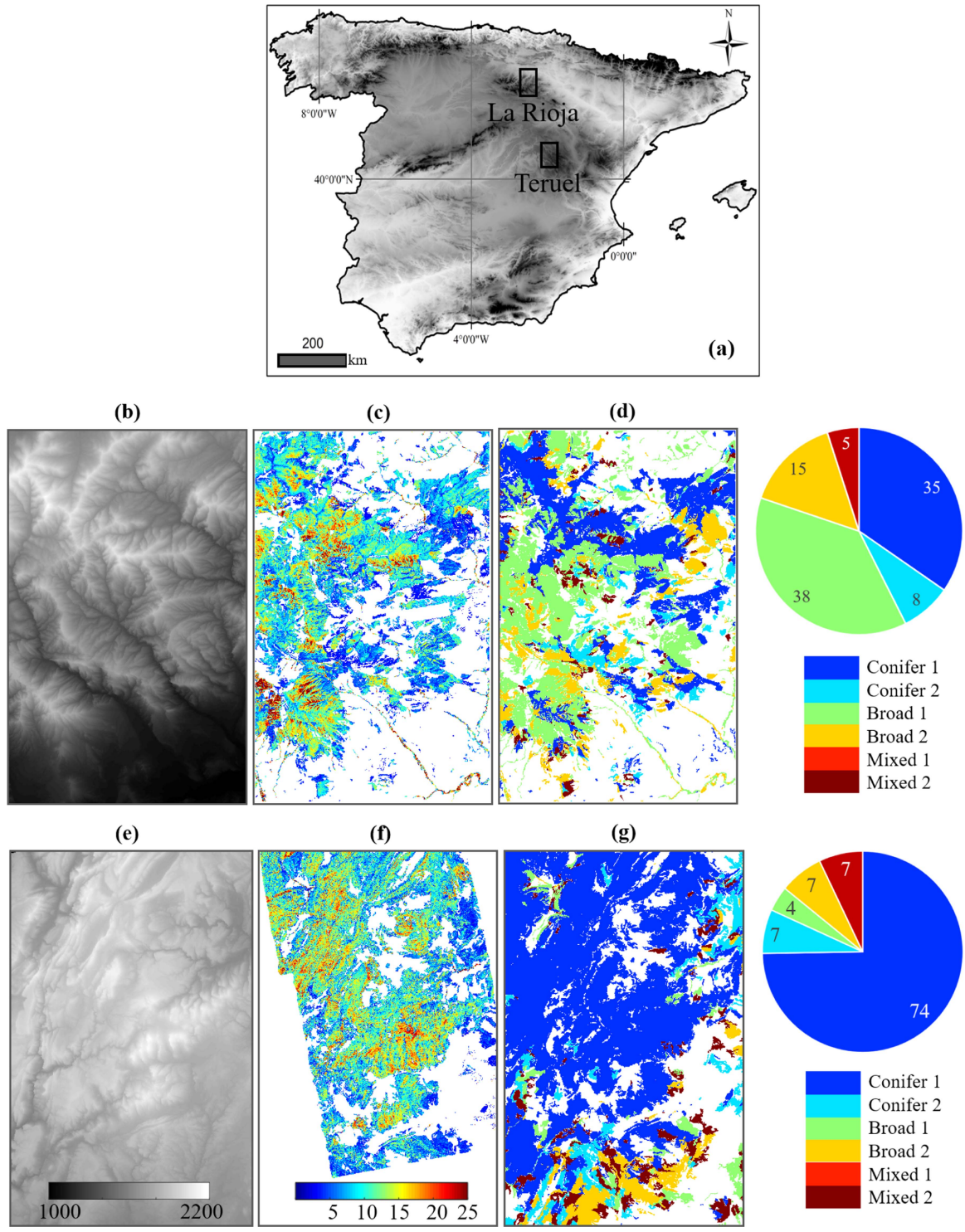

Fig. 1. Information of the study sites: La Rioja (middle) and Teruel (bottom). (a) Geographical location. (b) and (e) TanDEM-X DEM 90 m. (c) and (f) LiDAR forest height. (d) and (g) Forest type map and proportion.

to ensure that the estimated coherence can mitigate the bias in coherence estimation (as referenced by the average coherence reported in the XML file upon the release of the CoSSC data) and minimize the influence of topographic effects of variable topography or forest discontinuities [18], [36]. In this way, the accurate estimation for coherence enables the inversion of the actual forest height.

C. Airborne LiDAR Data

Precise airborne LiDAR data acquired in the framework of the Spanish National Territory Observation Program was used. The LiDAR data for forests are refreshed every six years, with a density of approximately 0.5 points per m^2 from 2009 to 2015 ($\pm$2 years), and a next version (in production stage) configured

TABLE II
INTRODUCTION OF CHARACTERISTIC PARAMETERS OF VEGETATION INDEX FROM OPTICAL REMOTE SENSING

Name	Calculation	Characteristic
NDVI	$\mathrm{NDVI}=\frac{b_{NIR}-b_R}{b_{NIR}+b_R}$	➢ The range is [-1, 1]. ➢ The negative value means that the observation target is water or covered by clouds, 0 means bare soil, while the larger the vegetation coverage, the closer to 1.
RVI	$\mathrm{RVI}=\frac{b_{NIR}}{b_R}$	➢ The range is [0, 30+]. ➢ The RVI of the vegetated area is much greater than 1, while that of the nonvegetated area is approximately 1. The more vegetated the area, the greater the value.
DVI	$\mathrm{DVI}=b_{NIR}-b_R$	➢ It is the difference between NIR and IR band, and sensitive to soil changes and short vegetation.
EVI	$\mathrm{EVI}=\frac{2.5*(b_{NIR}b_R)}{b_{NIR}+6*b_R-7.5*b_B+1}$	➢ The range is [-1,1]. ➢ Optimized NDVI, which is sensitive to the vegetation canopy structure.
FVC	$\mathrm{FVC}=\left[\frac{NDVI-NDVI_S}{NDVI_V+NDVI_S}\right]^2$	➢ The range is [0,1] as an important parameter representing vegetation coverage. ➢ The larger the vegetation coverage, the closer it is to 1.

b_{NIR} and b_R, respectively, represent the radiation values of near-infrared and infrared wavelengths, b_B is blue light radiation values, and NDVIs and NDVIv said bare soil area and vegetation area *NDVI* value.

with 1–14 points per m^2. There are little significant changes (deforestation or forest fires) and the impact of temporal discrepancy can be considered negligible. After data processing and transformation, a LiDAR forest height product with a resolution of 10 m, similar to that of the processed TanDEM-X InSAR data, is supplied as the reference data for validating the InSAR-derived forest height.

D. Optical Remote Sensing Data

In order to provide information related to forest density, structure, and coverage, optical data are exploited. Since many vegetation indices can represent differently the conditions of forests, a set of typical vegetation indices derived from optical remote sensing data was introduced to help distinguish the relationships between InSAR coherence and forest height. For this purpose, optical remote sensing images were used.

For the two study sites, due to the failure of the scan line corrector on Landsat-7 in May 2003, a loss of data strips occurred in the images acquired thereafter. This loss greatly impacted the usability of Landsat ETM remote sensing images [37]. Consequently, to deal with this issue, we utilized Landsat-8 images launched in March 2013, which were one year apart from the InSAR data and provides the optimal supplement. To extract more meaningful structural information, we collected three acquisitions of data within the same season with TanDEM-X InSAR data (leaf-off) and calculated the average value, ensuring the validity of the derived vegetation indices. Landsat-8 images from the same season as TanDEM-X InSAR data were selected, which could maintain the coincident similarity of vegetation attributes. In addition, the cloud in the image should be as little as possible to keep "visibility" in the forested area. Table II lists the vegetation indices used in this article [38].

E. Forest Inventory Data

The Spanish Forest Map (MFE50) was finished in 2012 for the whole country, including a forest-type map, a forest/nonforest map, and information at the stand level [39]. As an important database for defining areas with similar forest species and heights, it is updated every three years. In this article, forest inventory data were used to mask out nonforest areas and to validate the inversion results. The information for each forest type is listed in Table III [34], [39].

III. METHODOLOGY

A. SINC Function Model

From two SAR images simultaneously acquired by the TanDEM-X system, the observed coherence γ is computed. After removing all decorrelation factors unrelated to volume scattering [13], [18], [19], [20], the measured coherence can be effectively expressed by the RVoG model, which considers the volume and ground contribution as [23]

$$\tilde{\gamma}=e^{i\varphi_0}\,\frac{\gamma_\nu+\mu}{1+\mu} \tag{1}$$

where φ_0 is the ground phase and μ is the ground-to-volume amplitude ratio. γ_v is the volume coherence, directly related to the height of the forest h_v, extinction coefficient σ, and effective vertical wavenumber k_z, given by

$$\gamma_\nu=\frac{\int_0^{h_\nu} f(z)\,e^{ik_z z}dz}{\int_0^{h_\nu} f(z)\,dz}=\frac{2\sigma\left(e^{2\sigma h_\nu/cos\theta+ik_z h_v}-1\right)}{(2\sigma+ik_z\cos\theta)\left(e^{2\sigma h_\nu/\cos\theta}-1\right)} \tag{2}$$

$$k_z=\frac{2m\pi\Delta\theta}{\lambda\sin\theta}=\frac{2m\pi B_\perp}{\lambda R\sin\theta} \tag{3}$$

where θ is the incident angle of the electromagnetic wave, $\Delta\theta$ represents the difference in the incidence angle of the two radar images, λ denotes the radar wave operating wavelength, B is the baseline length, and $B_\perp$ is the vertical baseline. $f(z)$ is the function of the vertical structure, which is related to the extinction coefficient and canopy height. It should be noted that $m=1$ in bistatic mode and $m=2$ in monostatic mode for k_z [12], [23].

TABLE III
INFORMATION ON DIFFERENT FOREST TYPES, INCLUDING DOMINANT TREE SPECIES AND FOREST HEIGHT DISTRIBUTION

Order	ID	Forest Type	Dominant Species	Information
1	Conifer 1	Pines	*P. sylvestris, P. pinaster, P. nigra, P. pinea, P. halepensis, P. uncinta,*	➢ Evergreen coniferous forest ➢ Dense forest ➢ Average height ~10 m, maximum ~35 m
2	Conifer 2	Other coniferous	*Pinus spp., Juniperus spp.*	➢ Evergreen coniferous forest ➢ Density differs significantly ➢ Average height ~5 m, maximum ~15 m
3	Broad 1	Temperate broadleaf forest	*Quercus robur, Q. petraea, Fagus sylvatica*	➢ Winter-deciduous dominated ➢ Relatively high density ➢ Average height ~12 m, maximum ~33 m
4	Broad 2	Mediterranean broadleaf forest	*Fagus sylvatica, Betula spp., Fraxinus spp., Quercus ilex, Q. pyrenaica, Q. faginea, Q. suber*	➢ Evergreen broad-leaf forest dominates ➢ Density differs significantly ➢ Average height ~6 m, maximum ~28 m
5	Mixed 1	Coniferous mixed with temperate broadleaved	*Pinus spp., Quercus spp., Fagus sylvatica*	➢ Mixed of coniferous and broad-leaf forests ➢ Average height ~6 m, maximum ~18 m
6	Mixed 2	Coniferous mixed with Mediterranean broadleaved	*Pinus spp., Quercus spp.*	➢ Coniferous and Mediterranean forests are mixed ➢ Average height ~5 m, maximum ~15 m

Due to the limited penetration of the *X*-band, previous studies have shown that the inversion is effective when the ground scattering contribution in forested areas can be ignored, which means $\mu = 0$ [12], [29], [30]. In this case, the $\tilde{\gamma}$ can be directly represented by volume coherence γ_v, i.e.,

$$\underset{\mu \approx 0}{\tilde{\gamma}} = e^{i\varphi_0}\gamma_\nu = f(\varphi_0, h_v, \sigma). \tag{4}$$

The complex coherence provides two observations (interferometric phase and coherence amplitude), while there are three model unknowns, namely ground phase φ_0, forest height h_v, and extinction coefficient σ. Consequently, the equation is not balanced. If we assume that the extinction coefficient is zero, the following equation can be obtained [9]:

$$\lim_{\sigma \to 0} \gamma_\nu = \frac{e^{ik_z h_v} - 1}{ik_z h_v}. \tag{5}$$

With the help of a trigonometric transformation, the above equation can be written as

$$\tilde{\gamma} = e^{i\varphi_0}\ \gamma_\nu = e^{i\varphi_0}\ e^{ik_z h_v/2}\ \frac{\sin(k_z h_v/2)}{k_z h_v/2} = f(\varphi_0, h_v). \tag{6}$$

Equation (6) is known as the SINC model because the relation between coherence magnitude and vegetation height takes the form of a SINC function: $\sin(x)/x = \mathrm{sinc}(x)$. In addition, in (6), the scattering phase center height is located at half of the forest height. The complex coherence coefficient $\tilde{\gamma}$ depends on only the ground phase φ_0 and the forest height h_v. In addition, we can ignore the phase of the complex coherence and keep the amplitude only. In such a case, the coherence magnitude is a function of only h_v (unknown) and the system parameter k_z. Then, we can transform HoA to $2\pi/k_z$, and $|\gamma_v|$ can be expressed as

$$|\gamma_v| = \mathrm{sinc}\left(\frac{\pi h_v}{\mathrm{HoA}}\right). \tag{7}$$

According to the SINC model in (7), forest height can be estimated from the amplitude of TanDEM-X InSAR coherence directly.

B. Multi-SINC Model

The SINC model does not align with the assumptions that a null extinction coefficient and null ground-to-volume amplitude ratio in many forested areas since previous studies have shown that TanDEM-X has some penetrating ability [21]. Another critical problem hindering the robustness of the SINC model regarding its usability is that different InSAR pairs have special attributes, which means that a fixed function cannot describe the relationship between InSAR coherence and canopy height in different forest scenes, which means that the SINC model is not self-adaptive [29], [34].

A solution to this challenge is to employ semiempirical models, among which one representative model adds two parameters to the SINC model, which is now expressed as follows [29], [30], [34]:

$$|\gamma_v| = C_1\ \mathrm{sinc}\left(C_2 \frac{\pi h_v}{\mathrm{HoA}}\right). \tag{8}$$

In the above formula, C_1 and C_2 are two semiempirical parameters introduced to better adjust the relationship between coherence and forest height. Since C_1 and C_2 are two constants used as semiempirical parameters for certain interferometric pairs, this model is named as SeEm-SINC model [29], [30]. Fig. 2 shows the relationship between InSAR coherence and forest height for both the SINC model and the SeEm-SINC model.

To determine the appropriate semiempirical parameters C_1 and C_2, LiDAR forest height data in a subset area were selected as the true values. It is important to note that, although the effective vertical wavenumber has been estimated locally [40], [41], the presence of slopes changes the relationship between

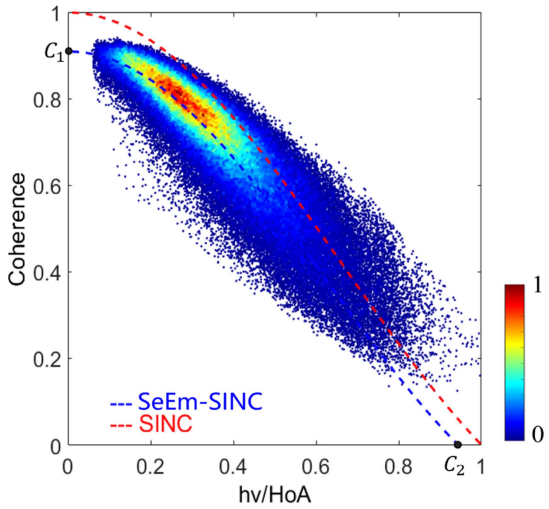

Fig. 2. Schematic diagram of the SINC model and SeEm-SINC model. The SINC model is represented by the red line, while the SeEm-SINC model is represented by the blue line.

the backscattered signal and the forest in the scene [40]. To ensure the robustness of the estimated parameters, pixels with range slopes outside the $(-5°, 5°)$ interval are excluded [34], [41]. Finally, the nonlinear least squares criterion is used as the constraint to determine the model parameters, expressed as

$$\min \left\| \text{RMSD} = \sqrt{\frac{\sum_{i=1}^{N} \left(\gamma_{v_i}^{\text{mod}} - \gamma_{v_i}^{\text{obs}}\right)^2}{N}} \right\} \quad \text{where}: C_1 \in [0.8,\ 1], C_2 \in [0.8, 2] \tag{9}$$

where $|\gamma_v| = C_1 \operatorname{sinc}\left(C_2 \frac{\pi h_v}{\text{HoA}}\right)$

where γ_v^{mod} and γ_v^{obs} represent the expected coherence from the model and the observed volume coherence, respectively. After establishing the SeEm-SINC model, it is considered that the forest attributes in the area covered by the InSAR image are similar, and then the canopy height could be directly inverted by the InSAR coherence.

The SeEm-SINC model incorporates two semiempirical parameters with the help of a small amount of LiDAR data, which makes the model adaptive to the forest scenario and the baseline configuration [42]. The correlation between InSAR coherence and forest height is preferred in this model than in the SINC function model, so it reduces certain systematic bias present in the SINC model to some extent [34]. However, in complex forest regions with severe topographic terrain, the relationship has multiple solutions rather than a one-to-one correspondence due to the variability of forest properties over the scene. As shown in Fig. 2, although the SeEm-SINC curve passes through the region with the highest density of point clouds, it can only represent the relationship of the majority of pixels, but many points are far from the model curve. As s result, many pixels located on steep slopes were not involved in the estimation of semiempirical parameters. Therefore, when estimating forest height from all pixels, more points fall away from the curve, which brings some unexpected errors.

The method proposed in this work to solve this issue consists of expanding the single SeEm-SINC model curve into more curves to form the so-called multi-SINC model.

There are several selections for establishing the multi-SINC model. First, slope should be considered as a crucial factor since it influences the relationship between forest height and InSAR coherence. In addition, forest type varies in the SeEm-SINC model, so we can establish the multi-SINC model by distinguishing different forest types. Another choice would be to consider all factors concurrently, as the multiple-solution relationship is caused by various elements, including slope, forest type, forest density, forest continuity, and forest coverage. From all possible options, in order to keep the multi-SINC model as simple as possible, the solution proposed in this work consists of adding two model curves, approximately parallel to the SeEm-SINC curve, and located above and below the existing curve. In this way, every pixel has a curve closer to it than with the single SeEm-SINC curve and, consequently, the inversion error can be reduced.

By denoting the semiempirical parameters of the upper curve as C_{1+} and C_{2+} and the semiempirical parameters of the lower curve as C_{1-} and C_{2-}, the mathematical expression of the multi-SINC model can be written as follows:

$$|\gamma_v| = \begin{cases} C_{1+}\operatorname{sinc}\left(C_{2+}\frac{\pi h_v}{\text{HoA}}\right) \\ C_1 \operatorname{sinc}\left(C_2 \frac{\pi h_v}{\text{HoA}}\right) \\ C_{1-}\operatorname{sinc}\left(C_{2-}\frac{\pi h_v}{\text{HoA}}\right). \end{cases} \tag{10}$$

The effectiveness of the SeEm-SINC curve lies in its ability to represent the relationship between coherence and canopy height in the majority of pixels, whereas the purpose of the two additional curves describes the relationship found in other pixels, which are far away from the SeEm-SINC curve. Based on this criterion, the values of the new semiempirical parameters are determined, as explained in Section III.

Fig. 3 depicts an example to illustrate both the SeEm-SINC model and the multi-SINC model. When establishing the SeEm-SINC model, only pixels with slopes between $-5°$ and $5°$ were exploited. It is shown that the distribution of pixels with all slopes has higher dispersion around the SeEm-SINC curve, so using a single SeEm-SINC model cannot properly represent all pixels. Instead, the use of three curves in the multi-SINC model helps consider better all points.

Regarding the criterion of the selection of the number of curves, we face a compromise between the solvability and practicality of the model, i.e., to improve the accuracy of the inversion and make the model solvable. In other words, if more curves (i.e., 5, 7, or more) relatively parallel to the SeEm-SINC were incorporated, the relationship between InSAR coherence and forest height could be more accurately characterized, but this goes against the solution convenience of the model, which means it is difficult to distinguish which curve each pixel belongs to.

C. Algorithm for Estimation of Forest Height

Many factors from both the system configuration (HoA, InSAR coherence, backscattering coefficient, and incidence angle)

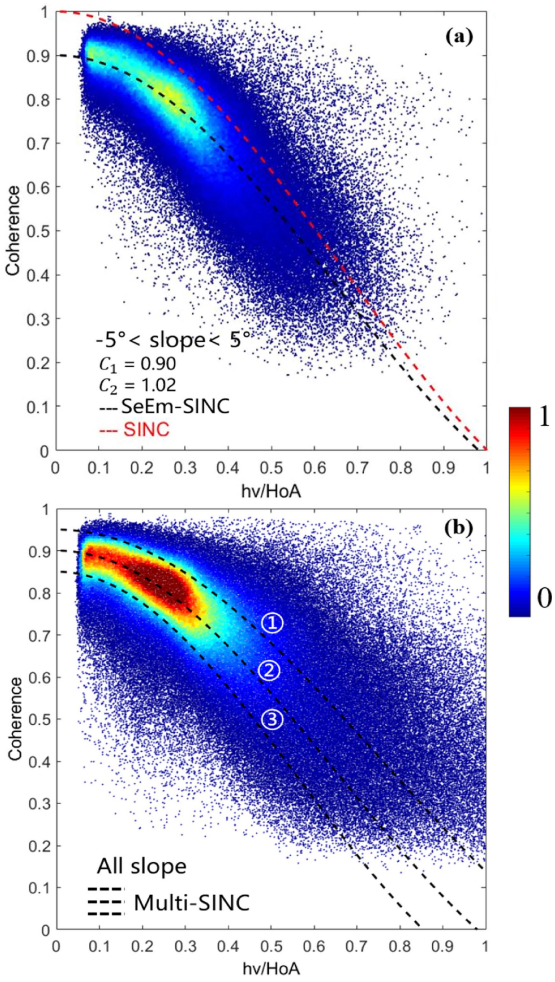

Fig. 3. Comparison of the schematic diagrams of the (a) SeEm-SINC model and (b) multi-SINC model.

and the forest scene (local slope, forest continuity, forest density, forest type, and horizontal distribution) affect the relationship between InSAR coherence and forest height. In view of the unclear resulting relationships, multisource remote sensing data are employed to provide the information required to estimate forest height adaptatively. Then, by using ML for training–verification–prediction, the goal is to distinguish which curve in the multi-SINC model should be chosen for each pixel in a wide area to minimize the overall error. The features employed as inputs for the ML algorithm come from different sources. The TanDEM-X InSAR data were used to provide features, such as coherence, HoA, backscattering coefficient, and incidence angle. The continuity and coverage (i.e., the horizontal distribution) over short and sparse forested areas [43], which varies importantly over the scene, are described by vegetation indices derived from optical remote sensing images. The Spanish forest map provides information on forest type. Finally, the multi-SINC model is established based on a subset of LiDAR forest height, which is employed as a reference. The implementation details are described in the next paragraphs, while a flowchart is presented in Fig. 4, and the strategies to be implemented are as follows.

1) Step 1. Data Preparation: The TanDEM-X InSAR observation is used to provide the coherence γ_v, the backscattering coefficients of the master and slave images m_1 and m_2, the height of ambiguity HoA , the local incidence angle θ_0, and the slope in range α. Landsat 8 optical remote sensing images are applied to extract the following vegetation indices: Normalized difference vegetation index (NDVI), ratio vegetation index (RVI), DVI, enhanced VI (EVI), and fractional vegetation cover (FVC). The forest type at each pixel was extracted from the MFE50 forest inventory data.

2) Step 2. Modeling of Multi-SINC: First, with the aid of the subset-area LiDAR forest height, except for the pixels with slopes greater than 20° that need to be masked since the extreme sloped areas bring unacceptable error, all pixels are involved in the drawing of the point cloud figure of the relationship between coherence and forest height normalized by HoA.

Then, the middle single SeEm-SINC curve is determined by fitting the two semiempirical parameters using the pixels with an absolute slope between $(-5°, 5°)$. In this way, SeEm-SINC model is built using (9) and the error caused by large slopes is avoided as much as possible.

Once we have settled the middle curve in the multi-SINC model, the next issue to address is how to determine the semiempirical parameters for the other two curves. In order to reasonably determine these semiparameters, we attempted forest height inversion using multiple sets of semiempirical parameters with assistance from the subarea of LiDAR data. We compared the results with LiDAR forest height and selected the set of parameters that yielded the highest accuracy as the semiempirical parameters to form the multi-SINC model.

3) Step 3. Mapping of Forest Height: For the selected subset area, three curves in the multi-SINC model are used to invert the forest height for every pixel, and the curve with the minimum error is selected to label each pixel with a curve index (i.e., 1, 2, or 3). Hence, each pixel is characterized by a total of 12 features, i.e., γ_v, m_1, m_2, HoA, θ_0, α, NDVI, RVI, EVI, DVI, FVC, forest type, and a label.

Random forest is a classic and efficient ML method with excellent performance in classification problems. In fact, it has been previously applied to InSAR/PolInSAR forest parameter inversion [44], [45], [46], [47], [48]. Therefore, the random forest algorithm is adopted in this work to classify the pixels into the three possible curves. The subset area with LiDAR data is used for training. Regarding the estimation in the rest of the scene, predicted labels based on the above 12 features are exploited to classify and solve the multi-SINC model. Finally, LiDAR forest height over the whole scene is applied for validation and analysis.

IV. Results

A. Modeling Results

We used the proposed method to explore various combinations of semiempirical parameters in order to form a multi-SINC model. With the assistance of subset-area LiDAR forest height data, we were able to identify the optimal combination of

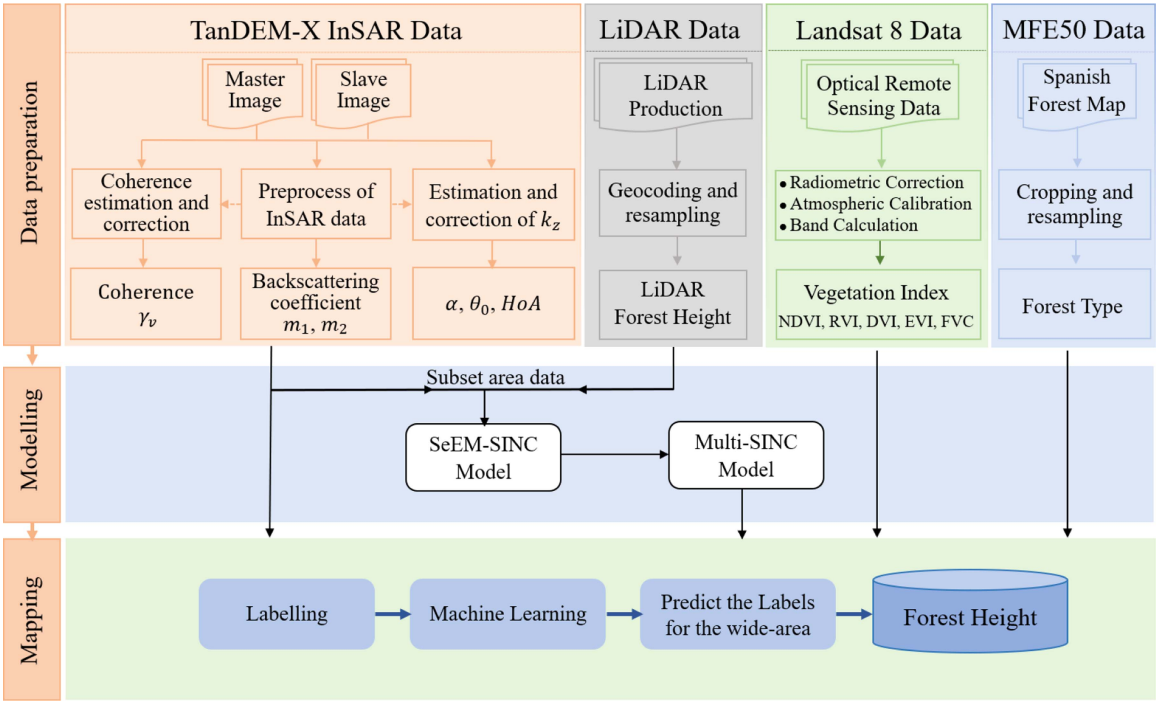

Fig. 4. Flowchart of forest height inversion based on the multi-SINC model.

TABLE IV
PROCESS OF OPTIMIZING THE DIFFERENT COMBINATIONS OF SEMIEMPIRICAL PARAMETERS IN MULTI-SINC MODEL (LA RIOJA STUDY SITE)

Order	C_{1+}	C_{2+}	C_1	C_2	C_{1-}	C_{2-}	RMSE (m)
1	0.92	0.96	0.90	1.02	0.88	1.08	1.94
2	0.93	0.93			0.87	1.11	1.62
3	0.94	0.90			0.86	1.14	1.39
4	0.95	0.87			0.85	1.17	1.25
5	0.96	0.84			0.84	1.20	**1.18**
6	0.97	0.81			0.83	1.23	1.21
7	0.98	0.78			0.82	1.26	1.26
8	0.99	0.75			0.81	1.29	1.39

semiempirical parameters. To illustrate the optimization process, we selected the La Rioja study site as an example and the results are presented in Table IV. From Table IV, it was observed that the inversion accuracy is optimal when the fifth group of semiempirical parameters is employed. Therefore, the multi-SINC model, corresponding to the fifth group of semiempirical parameters, can be utilized to invert forest height in the La Rioja study site.

As a result, multi-SINC models were established for the two study sites. The curves of the multi-SINC model established at the two study sites are shown in Fig. 5.

When fitting the parameters of the SeEm-SINC model, to avoid the influence of topography, only local range slopes within $\pm 5^\circ$ are retained for parameter estimation, which makes the point clouds more clustered around the SeEm-SINC curve. In the representation of the three curves of the multi-SINC model,

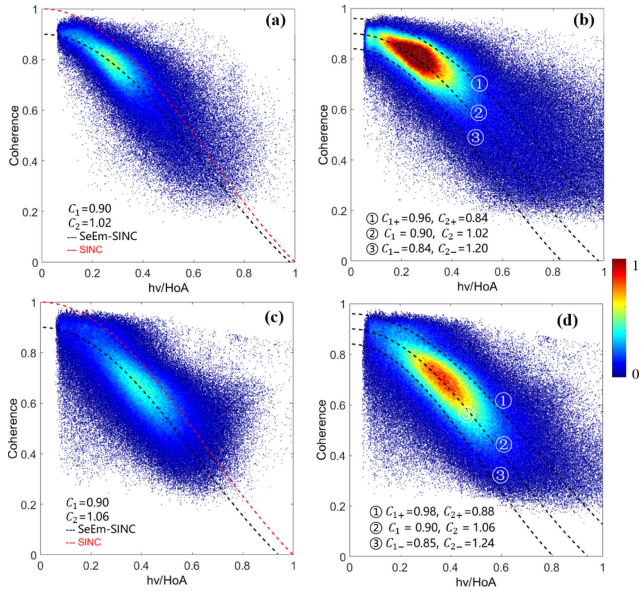

Fig. 5. Modeling result in the two study sites with the assistance of a subset-area LiDAR forest height. (a) SeEm-SINC model and (b) multi-SINC model in La Rioja study site. (c) SeEm-SINC model and (d) multi-SINC model in Teruel study site.

the density is wider than that of the SeEm-SINC model because the slope span is $\pm 20^\circ$ now, and this is observed at both study sites. By extending a single curve to three relatively parallel curves, the multi-SINC model can basically cover the region of points with higher density. In addition, the relationship between the InSAR coherence and LiDAR forest height in all slopes was drawn in the diagram of point cloud, showing that the core region is denser than the SeEm-SINC curve diagram within slopes

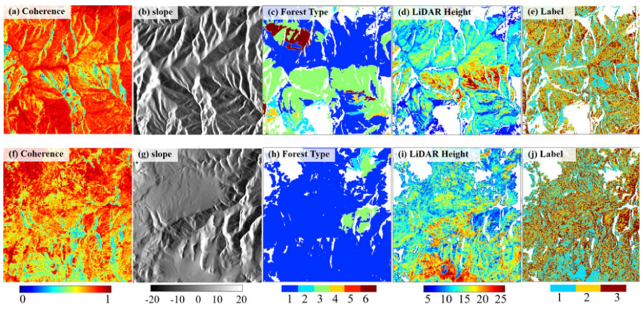

Fig. 6. Input features and results of the labeling in the training areas in La Rioja (a)–(e) and Teruel (f)–(j) study sites. (a) and (f) InSAR coherence. (b) and (g) Slope. (c) and (h) Forest type. (d) and (i) LiDAR forest height. (e) and (j) Resulting label.

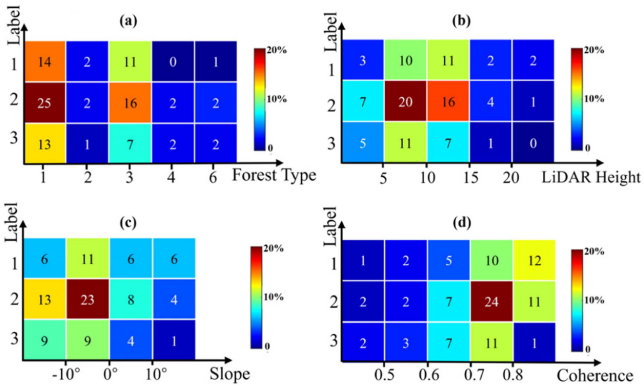

Fig. 7. Proportion of the different labels for each feature, including (a) forest type, (b) LiDAR forest height, (c) slope, and (d) InSAR coherence (taking the La Rioja study site as the example). (a) Label vs. forest type. (b) Label vs. LiDAR height. (c) Label vs. slope. (d) Label vs. coherence.

ranging $\pm 5^{\circ}$. The critical reason is that in the large slope region outside $\pm 5^{\circ}$, there are also numerous pixels meeting or close to the SeEm-SINC curve, which confirms the multiple-solution relationship between InSAR coherence and canopy height.

After the multi-SINC model is established, all pixels of the subset area with LiDAR forest height data are labeled with a 1, 2, or 3, associated with the three curves of the multi-SINC model. For this purpose, the classification refers to the set of 12 input features available and the minimum difference between the LiDAR forest height and the height estimates retrieved by the multi-SINC model curves. The results of the labeling are shown in Fig. 6.

As shown in Fig. 6, the distribution of labels presents the randomness overall, and no obvious rule can be visually found. In order to analyze it further, we have obtained the proportion of each label corresponding to forest type, LiDAR forest height, slope intervals, and InSAR coherence, and the results are shown in Fig. 7. In general, Label 2 is the most represented label because it represents the central curve of the model, which accounts for more pixels (more density in the scatter plots) than the other two curves. In addition, on the whole, label classification shows randomness for every feature, which suggests that the label cannot be determined by any single feature. In other words, the comprehensive influence of multiple features determines the relationship between InSAR coherence and forest height.

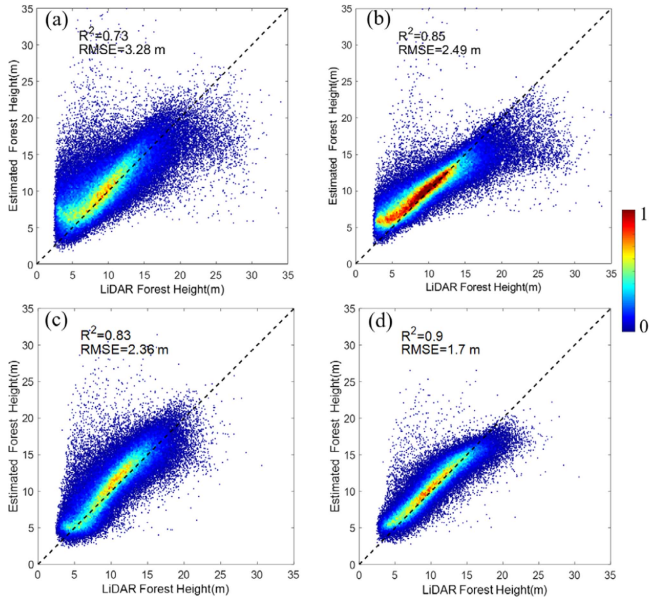

Fig. 8. Validation of forest height inversion results. (a) Result from SeEm-SINC model in La Rioja. (b) Result from multi-SINC model in La Rioja. (c) Result from SeEm-SINC model in Teruel. (d) Result from multi-SINC model in Teruel.

B. Forest Height Mapping and Validation

Using the subset-area data labeled above, along with the 12 features provided by the existing remote sensing data from multiple sources, equal proportions of samples were selected for training (50%) and verification (50%) by random forest, and the trained model was output for classifying and predicting the labels of all interferometric images. Finally, the multi-SINC model was exploited to invert forest height according to the predicted labels all over the scene.

To make sense of the performance of the new method, the same statistical scale with a window size of 10×10 as a plot, approximately 0.7 hectares, was used to validate the accuracy, and the results are shown in Fig. 8. Compared with the SeEm-SINC model, the cloud of points of the multi-SINC model is closer to the line $y = x$. An overestimation present in the SeEm-SINC model for the low-forest area is effectively suppressed by the multi-SINC model. Especially for areas with shorter trees, the overestimation coursed by the SeEm-SINC model was greatly improved. The RMSEs of the two study sites were improved to 2.49 m and 1.7 m, instead of 3.28 m and 2.36 m from the SeEm-SINC model, respectively.

The performance of the SINC model, the SeEm model, and the multi-SINC model over the two study sites is represented in Table V. The RMSEs of the SeEm-SINC model are more than 40% better than that of the SINC function model, and approximately 25% for the new method in this article is further improved, which is an acceptable performance for a complex area with short and sparse forests in Spain. The forest height maps are shown in Fig. 9. The maps of forest height show clear similarity to the LiDAR production. An advantage of the new method is that the overestimation or underestimation can be suppressed to some extent for lower or taller trees.

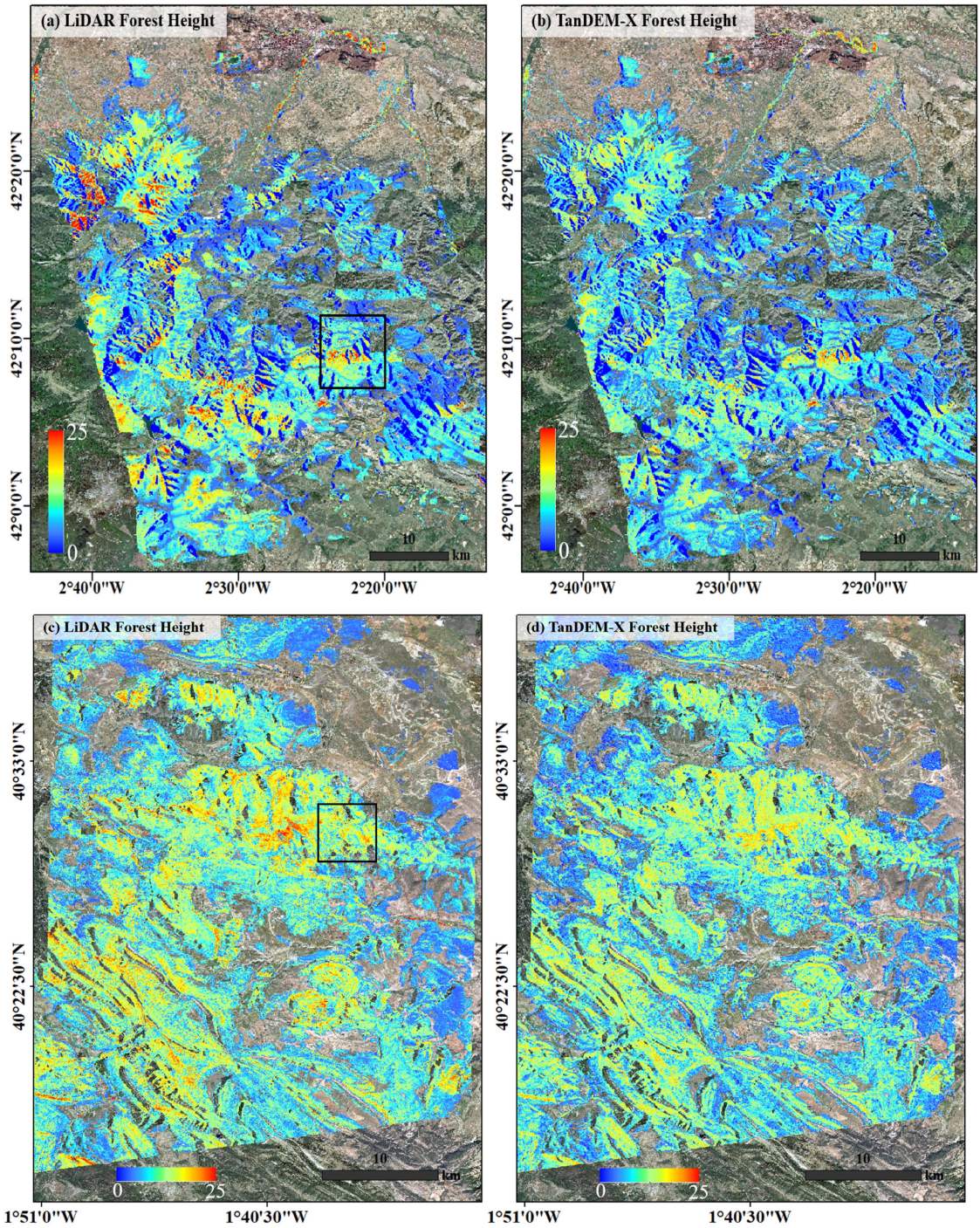

Fig. 9. Mapping result of forest height in (a) and (b) La Rioja and (c) and (d) Teruel, and the black rectangles are used to aid in modeling.

TABLE V
RMSEs AND R^2 VALUES OF FOREST HEIGHT INVERSION RESULTS USING DIFFERENT METHODS AT TWO STUDY SITES

Method	La Rioja		Teruel	
	RMSE (m)	R^2	RMSE (m)	R^2
SINC model	5.74	0.54	4.82	0.66
SeEm-SINC model	3.28	0.73	2.36	0.83
Multi-SINC model	2.49	0.85	1.70	0.90

There are also some factors leading to the remaining errors, which are commented in the following text. The proposed method is still derived from the SINC model, which by definition entails some error because of the assumptions of null extinction coefficient and ground-to-volume ratio. The slope is still one of the key factors limiting the accuracy, although an objective of the method proposed in this article was to constrain the many-to-one correspondence between the observed coherence and canopy height induced by slope. Finally, the forest type by itself is not a single characterization of the forests since each type of tree

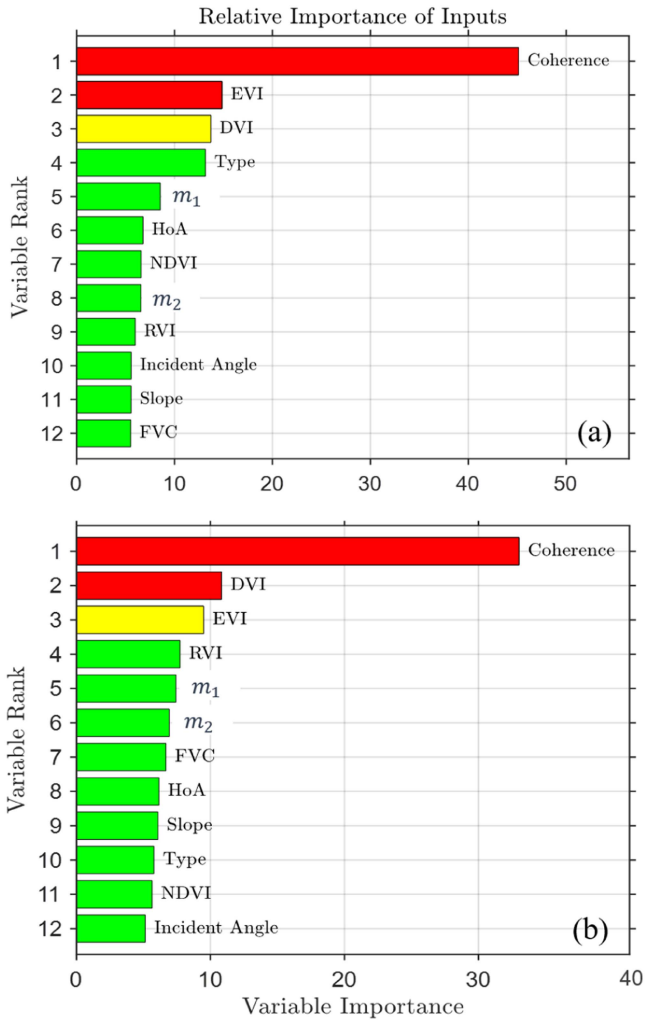

Fig. 10. Relative importance of features when ML is applied to (a) La Rioja and (b) Teruel.

species exhibits notable differences in canopy height, growth characteristics, density, and other aspects.

V. Discussion

A. Importance of the Features

The relative influence of each feature considered in the ML approach for the construction of training models is characterized by its importance, which is output from a random forest algorithm. The relative importance of all features at the two study sites is shown in Fig. 10. In general, the relative importance of the factors at the two study sites is similar, and so is their ordering. Among them, InSAR coherence is the leading influential factor, which plays a vital role in the process of label classification since it is directly derived from the coherence and LiDAR forest height. Then, two optical vegetation indices DVI and EVI present the second or third highest importance, with different orders at the two study sites. It should be noted that there is a clear difference in the importance of forest type at the two study sites. It is the fourth feature in La Rioja, whereas it is the tenth in Teruel. The reason lies in the different proportions of forest type in the two sites. In the La Rioja site, there is a large proportion of various types (37%, 35%, 15%, etc.) but in the Teruel site, a single forest type (Conifer 1) corresponds to 74% of the area. Therefore, when the forest species present in a certain area are diverse, forest type makes a greater contribution to ML than when a single type is dominant.

B. Necessity of Using Multiple Features

In the research carried out to improve the results provided by the SeEm-SINC model, we originally focused on two individual key factors that were considered relevant and which could lead to the construction of multi-SINC models based only upon them: slope and forest type. In this section, taking the La Rioja study site as an example, we analyze the performance of the multi-SINC model when only a single feature is considered to define the multiple curves.

First, the slope is known to affect the compliance of the assumptions of the SINC-based models: null ground-to-volume ratio and null extinction. With this in mind, the range slopes were divided into several intervals and (9) was used as the criterion to obtain a different SeEm-SINC model for each slope interval. The obtained SeEm-SINC models of each slope interval are shown in Fig. 11. There are obvious differences in the fitted semiempirical parameters (from 0.86 to 0.92 in C_1, and from 0.71 to 1.03 in C_2).

The results obtained for the two curves within $\pm 10^\circ$ are close to the curve obtained when only $\pm 5^\circ$ pixels are used since they are relatively flat areas. However, there are many pixels represented better by any of the other four curves than by the curve obtained with only the $\pm 5^\circ$ interval of slopes. All the curves are drawn in the same plot in Fig. 11(f). It is clear that, although there are important differences in the semiempirical parameters obtained for each curve, in the region with a short forest, there is much overlap among the curves. In the La Rioja study site, the tree heights are mostly concentrated between 0.1 and 0.5 times the HoA. Therefore, the use of different models based only on the slope interval would not change the final height estimation and its accuracy.

Similarly, a set of SeEm-SINC models is established for different forest types to invert the canopy height. To this aim, the slopes are limited to a relatively flat area (within $\pm 5^\circ$). The fitted semiempirical parameters are very similar for all forest types except for Conifer 2. This results in a challenge in distinguishing them effectively, as depicted in Fig. 12. When the five curves are plotted in Fig. 12(f), it is clear that there is an overlap. As a result, as in the case of using only slope as a feature to define the multi-SINC model, no improved performance is expected from this option.

The results from forest height inversion using the multi-SINC model, involving only a single feature (slope or forest type), yielded RMSE values of 4.16 m and 3.86 m, respectively, which are worse than the performance of the existing SeEm-SINC model (RMSE = 3.28 m). Obviously, regardless of whether the inversion considers slope or forest species only, compared with the comprehensive consideration of multiple factors, there is no advantage and the accuracy drops dramatically.

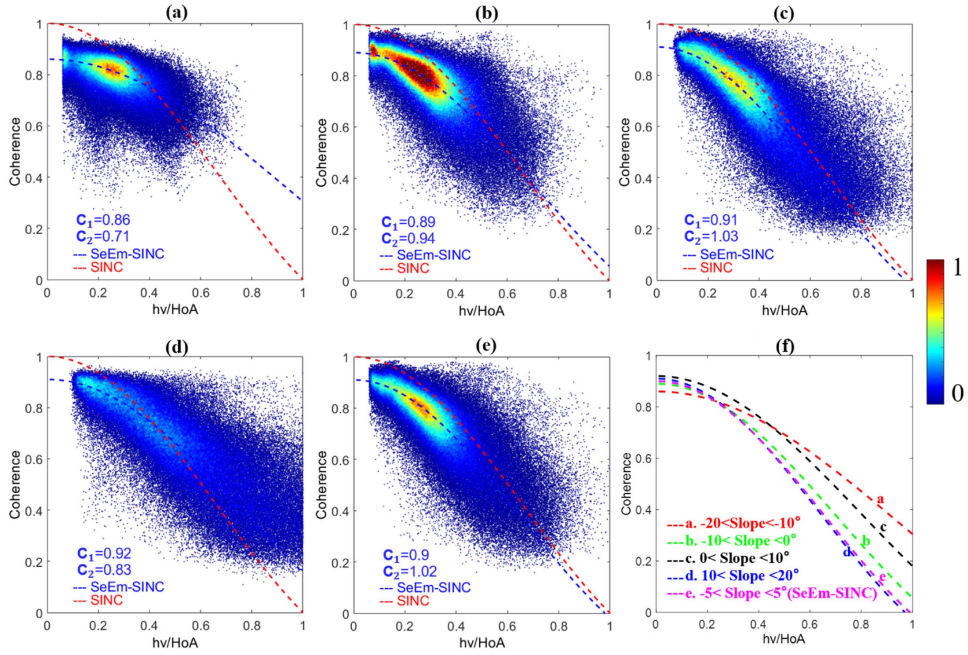

Fig. 11. Fitting results of semiempirical parameters for considering forest type only in La Rioja. (a) $-20^\circ <$ Slope $<-10^\circ$. (b) $-10^\circ <$ Slope $< 0^\circ$. (c) $0^\circ <$ Slope $<10^\circ$. (d) $10^\circ <$ Slope $< 20^\circ$. (e) $-5^\circ <$ Slope $< 5^\circ$ (SeEm-SINC). (f) All curves.

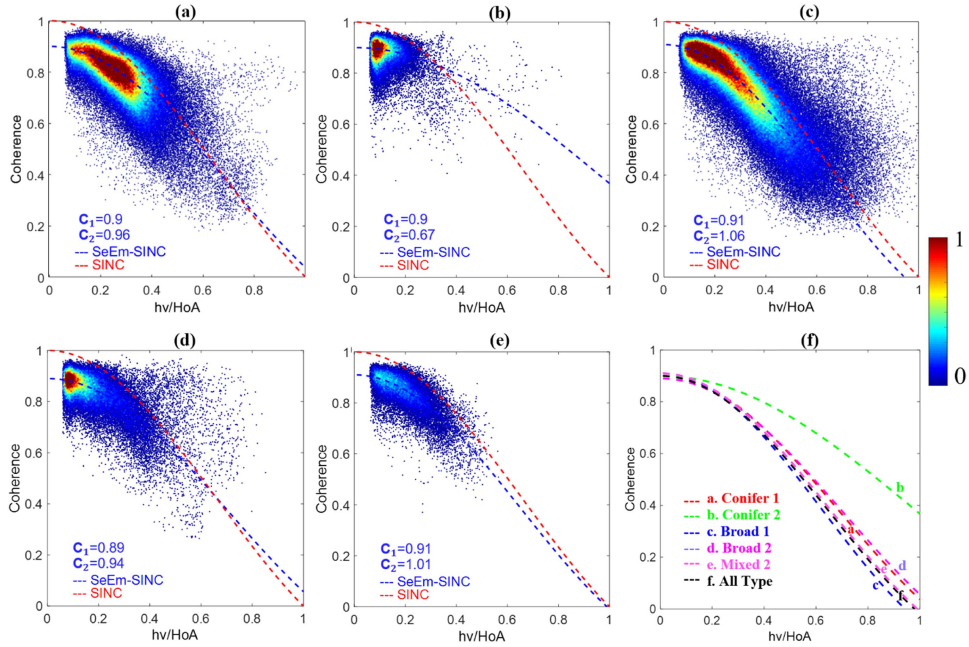

Fig. 12. Fitting results of semiempirical parameters for considering forest type in La Rioja, and the slope is limited to the range of $\pm 5^\circ$ to reduce its impact. (a) Conifer 1. (a) Conifer 2. (c) Broad 1. (d) Broad 2. (d) Mixed 2. (f) All curves.

Compared with the model that considers slope or forest type only, the advantage of the multi-SINC model proposed here, which considers multiple features, is that the contribution of various factors will make the coherence and forest height better correlated, and the contribution of each feature is a priori unknown in any pixel of the scene. Consequently, the multi-SINC model considering multiple features would be the preferable selection.

To comprehensively evaluate the performance of various datasets in addressing multi-SINC models, we carried out experiments in three distinct scenarios, grounded in the nature of features employed during ML training. This was necessitated by the unavailability of accurate forest type derived from forestry inventory data.

1) *Case A:* Using SAR observation data (coherence, HoA, backscattering coefficient from master and slave images,

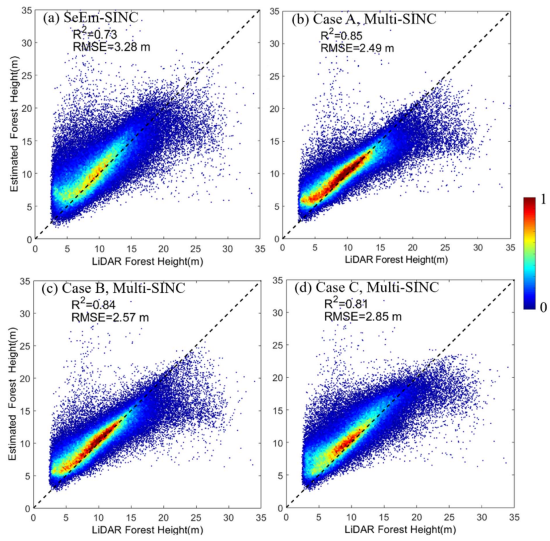

Fig. 13. Validation of forest height inversion results of different cases in multi-SINC model in La Rioja. (a) SeEm-SINC model. (b) Case A, multi-SINC model. (c) Case B, multi-SINC model. (d) Case C, multi-SINC model.

local incident angle, and range slope), vegetation indices derived from optical remote sensing data (NDVI, DVI, EVI, RVI, and FVC), and forest types from forestry inventory.

2) *Case B:* Using SAR observations and vegetation indices from optical data.
3) *Case C:* Using SAR observations only.

Taking the La Rioja study site as an example, we tested the performance of forest height inversion based on the multi-SINC model under the three cases. The validated results are shown in Fig. 13. The following points can be concluded.

1) The results obtained from the features extracted using the three types of data were optimal, with an RMSE of 2.49 m.
2) After removing the forest-type feature extracted from forestry surveys, the accuracy only decreased slightly. Given the challenges associated with obtaining precise forestry survey data and the limitations it poses on method transferability, the proposed method, which does not rely on forest-type data derived from forestry surveys, can still maintain great performance.
3) When only using features extracted from SAR observations, the results were only slightly better than those of the SeEm-SINC model.

To sum up, considering the effective role and easy availability of vegetation indices derived from optical remote sensing data in inversion, we suggest that combining features from TanDEM-X InSAR data and vegetation indices derived from optical remote sensing is a favorable choice.

C. Advantages and Limitations of the New Method

So far, many methods for retrieving forest height from TanDEM-X data have been verified in different forest scenarios (e.g., tropical rainforest, boreal forest, etc.). In the absence of external accurate DTM data, the method proposed in this article can retrieve forest height using only the InSAR coherence of TanDEM-X. The slope of forested area for complex terrain makes the relationship between InSAR coherence and forest height uncertain. The multi-SINC model is used to improve the accuracy with the help of ML. The effectiveness of the new method is proved at two study sites. Compared with those of the existing SINC model-based and semiempirical methods, the inversion accuracy is further improved [22], [23], [27]. To solve the problem of deviation between TanDEM-X InSAR coherence and forest height, our current correction is nonlinear rather than systematic, and the estimation method of the semiempirical parameters of the inversion model is clear. Furthermore, the method proposed in this article mitigates the random error to a certain extent.

We must admit that there are still limitations in the method proposed in this article, which should be further explored in future studies. The airborne high-precision LiDAR forest height product is employed as an assist. However, some previous studies have used external LiDAR DTM or canopy height model (CHM) products to assist the inversion [22], [27]. In addition, when previous studies used the existing LiDAR CHM data to retrieve forest height, they often only carried out a systematic correction, which cannot match the requirement for high-precision inversion, whereas the method proposed in this article can reduce random errors to a certain extent. Certainly, in the case of large-scale inversion, we still face the situation that high-precision airborne LiDAR products are not available everywhere.

VI. Conclusion

This work constitutes a proof-of-concept of a methodology to estimate forest height from TanDEM-X data based on the extension of the SeEm-SINC model by adding two nearly parallel curves. In this way, the inversion is carried out with the curve most adapted to each pixel, for which a set of 12 features (derived from multiple sources of data, including optical imagery, forest-type inventory, etc.) are exploited by an ML approach.

Results confirm that the inversion of forest height based on the multi-SINC model can effectively suppress much of the error in the SeEm-SINC model. Therefore, the performance of the forest height inversion is improved to some extent by integrating vegetation features derived from optical remote sensing data, TanDEM-X InSAR observations, and a small amount of LiDAR data. Faced with the challenges associated with obtaining accurate forestry inventory data, the proposed method can maintain a satisfactory performance without forest type from forestry inventory.

Although the method proposed in this article brings about some improvement, additional work will be carried out to improve the forest height retrieval and to extend it to forests in other geographical locations (e.g., boreal and tropical).

Acknowledgment

The authors would like to thank the German Aerospace Center (DLR) for providing all the TanDEM-X data under Project OTHER7349, the Spanish CNIG for making LiDAR data from

the PNOA freely accessible, and the Spanish MITECO for making the Spanish Forest Map freely accessible.

REFERENCES

[1] T. L. Toan, S. Quegan, M. W. J. Davidson, H. Balzter, and L. Ulander, "The BIOMASS mission: Mapping global forest biomass to better understand the terrestrial carbon cycle," *Remote Sens. Environ.*, vol. 115, no. 11, pp. 2850–2860, 2011.

[2] S. Quegan et al., "The European space agency BIOMASS mission: Measuring forest above-ground biomass from space," *Remote Sens. Environ.*, vol. 227, pp. 44–60, 2019, doi: 10.1016/j.rse.2019.03.032.

[3] S. Solberg, R. Astrup, J. Breidenbach, B. Nilsen, and D. Weydahl, "Monitoring spruce volume and biomass with InSAR data from TanDEM-X," *Remote Sens. Environ.*, vol. 139, pp. 60–67, 2013, doi: 10.1016/j.rse.2013.07.036.

[4] T. Markus et al., "The ice, cloud, and land elevation Satellite-2 (ICESat-2): Science requirements, concept, and implementation," *Remote Sens. Environ.*, vol. 190, pp. 260–273, 2017, doi: 10.1016/j.rse.2016.12.029.

[5] R. Dubayah et al., "The global ecosystem dynamics investigation: High-resolution laser ranging of the Earth's forests and topography," *Sci. Remote Sens.*, vol. 1, 2020, Art. no. 100002, doi: 10.1016/j.srs.2020.100002.

[6] L. Chen et al., "Improved estimation of forest stand volume by the integration of GEDI LiDAR data and multi-sensor imagery in the Changbai mountains mixed forests ecoregion (CMMFE), Northeast China," *Int. J. Appl. Earth Observ. Geoinf.*, vol. 100, 2021, Art. no. 102326, doi: 10.1016/j.jag.2021.102326.

[7] R. N. Treuhaft, S. N. Madsen, M. Moghaddam, and J. J. van Zyl, "Vegetation characteristics and underlying topography from interferometric radar," *Radio Sci.*, vol. 31, no. 6, pp. 1449–1485, 1996, doi: 10.1029/96rs01763.

[8] R. Bamler and P. Hartl, "Synthetic aperture radar interferometry," *Inverse Problems*, vol. 14, no. 4, pp. R1–R54, 1998.

[9] S. R. Cloude and K. P. Papathanassiou, "Polarimetric SAR interferometry," *IEEE Trans. Geosci. Remote Sens.*, vol. 36, no. 5, pp. 1551–1565, Sep. 1998.

[10] K. Papathanassiou and S. R. Cloude, "Single-baseline polarimetric SAR interferometry," *IEEE Trans. Geosci. Remote Sens.*, vol. 39, no. 11, pp. 2352–2363, Nov. 2001.

[11] S. R. Cloude and K. P. Papathanassiou, "Three-stage inversion process for polarimetric SAR interferometry," *IEE Proc. - Radar, Sonar Navig.*, vol. 150, no. 3, pp. 125–134, 2003.

[12] S. Cloude, *Polarisation: Applications in Remote Sensing*. Oxford, U.K.: Oxford Univ. Press, 2010.

[13] S. K. Lee, F. Kugler, K. P. Papathanassiou, and I. Hajnsek, "Quantification of temporal decorrelation effects at L-band for polarimetric SAR interferometry applications," *IEEE J. Sel. Topics Appl. Earth Observ. Remote Sens.*, vol. 6, no. 3, pp. 1351–1367, Jun. 2013.

[14] G. Krieger et al., "TanDEM-X: A satellite formation for high-resolution SAR interferometry," *IEEE Trans. Geosci. Remote Sens.*, vol. 45, no. 11, pp. 3317–3341, Nov. 2007, doi: 10.1109/tgrs.2007.900693.

[15] J. H. Gonzalez, M. Bachmann, G. Krieger, and H. Fiedler, "Development of the TanDEM-X calibration concept: Analysis of systematic errors," *IEEE Trans. Geosci. Remote Sens.*, vol. 48, no. 2, pp. 716–726, Feb. 2010, doi: 10.1109/tgrs.2009.2034980.

[16] P. Rizzoli et al., "Generation and performance assessment of the global TanDEM-X digital elevation model," *ISPRS J. Photogramm. Remote Sens.*, vol. 132, pp. 119–139, 2017, doi: 10.1016/j.isprsjprs.2017.08.008.

[17] M. Zink et al., "TanDEM-X: 10 years of formation flying bistatic SAR interferometry," *IEEE J. Sel. Topics Appl. Earth Observ. Remote Sens.*, vol. 14, pp. 3546–3565, Feb. 2021, doi: 10.1109/jstars.2021.3062286.

[18] M. Martone, B. Bräutigam, P. Rizzoli, C. Gonzalez, M. Bachmann, and G. Krieger, "Coherence evaluation of TanDEM-X interferometric data," *ISPRS J. Photogramm. Remote Sens.*, vol. 73, pp. 21–29, 2012, doi: 10.1016/j.isprsjprs.2012.06.006.

[19] M. Martone, B. Brautigam, and G. Krieger, "Quantization effects in TanDEM-X data," *IEEE Trans. Geosci. Remote Sens.*, vol. 53, no. 2, pp. 583–597, Feb. 2015, doi: 10.1109/tgrs.2014.2325976.

[20] P. Rizzoli, L. Dell'Amore, J.-L. Bueso-Bello, N. Gollin, D. Carcereri, and M. Martone, "On the derivation of volume decorrelation from TanDEM-X bistatic coherence," *IEEE J. Sel. Topics Appl. Earth Observ. Remote Sens.*, vol. 15, pp. 3504–3518, Apr. 2022, doi: 10.1109/jstars.2022.3170076.

[21] F. Kugler, D. Schulze, I. Hajnsek, H. Pretzsch, and K. P. Papathanassiou, "TanDEM-X Pol-InSAR performance for forest height estimation," *IEEE Trans. Geosci. Remote Sens.*, vol. 52, no. 10, pp. 6404–6422, Oct. 2014, doi: 10.1109/tgrs.2013.2296533.

[22] A. Olesk, K. Voormansik, A. Vain, M. Noorma, and J. Praks, "Seasonal differences in forest height estimation from interferometric TanDEM-X coherence data," *IEEE J. Sel. Topics Appl. Earth Observ. Remote Sens.*, vol. 8, no. 12, pp. 5565–5572, Dec. 2015, doi: 10.1109/jstars.2015.2501648.

[23] F. Kugler, L. Seung-Kuk, I. Hajnsek, and K. P. Papathanassiou, "Forest height estimation by means of pol-InSAR data inversion: The role of the vertical wavenumber," *IEEE Trans. Geosci. Remote Sens.*, vol. 53, no. 10, pp. 5294–5311, Oct. 2015, doi: 10.1109/tgrs.2015.2420996.

[24] R. N. Treuhaft et al., "The ambiguity in forest profiles and extinction estimated from multibaseline interferometric SAR," *Boletim Ciências Geodésicas*, vol. 15, no. 3, pp. 299–312, 2009.

[25] G. H. X. Shiroma and M. Lavalle, "Digital terrain, surface, and canopy height models from InSAR backscatter-height histograms," *IEEE Trans. Geosci. Remote Sens.*, vol. 58, no. 6, pp. 3754–3777, Jun. 2020.

[26] Y. Lei, R. Treuhaft, and F. Goncalves, "Tropical forest height and underlying topography from TanDEM-X SAR interferometry," in *Proc. IEEE Int. Geosci. Remote Sens. Symp.*, 2020, pp. 4979–4982.

[27] Y. Lei, R. Treuhaft, and F. Gonçalves, "Automated estimation of forest height and underlying topography over a Brazilian tropical forest with single-baseline single-polarization TanDEM-X SAR interferometry," *Remote Sens. Environ.*, vol. 252, 2021, Art. no. 112132, doi: 10.1016/j.rse.2020.112132.

[28] R. Treuhaft et al., "Tropical-forest biomass estimation at X-band from the spaceborne TanDEM-X interferometer," *IEEE Geosci. Remote Sens. Lett.*, vol. 12, no. 2, pp. 239–243, Feb. 2015, doi: 10.1109/lgrs.2014.2334140.

[29] H. Chen, S. R. Cloude, and D. G. Goodenough, "Forest canopy height estimation using TanDEM-X coherence data," *IEEE J. Sel. Topics Appl. Earth Observ. Remote Sens.*, vol. 9, no. 7, pp. 3177–3188, Jul. 2016, doi: 10.1109/jstars.2016.2582722.

[30] A. Olesk, J. Praks, O. Antropov, K. Zalite, T. Arumäe, and K. Voormansik, "Interferometric SAR coherence models for characterization of hemiboreal forests using TanDEM-X data," *Remote Sens.*, vol. 8, no. 9, 2016, Art. no. 700, doi: 10.3390/rs8090700.

[31] H. Q. Fu, J. J. Zhu, C. C. Wang, R. Zhao, and Q. H. Xie, "Underlying topography estimation over forest areas using single-baseline InSAR data," *IEEE Trans. Geosci. Remote Sens.*, vol. 57, no. 5, pp. 2876–2888, May 2019, doi: 10.1109/tgrs.2018.2878357.

[32] H. Wang et al., "Estimation of subcanopy topography based on single-baseline TanDEM-X InSAR data," *J. Geodesy*, vol. 95, no. 7, Jul. 2021, Art. no. 84, doi: 10.1007/s00190-021-01519-3.

[33] S.-K. Lee, T. E. Fatoyinbo, D. Lagomasino, E. Feliciano, and C. Trettin, "Multibaseline TanDEM-X mangrove height estimation: The selection of the vertical wavenumber," *IEEE J. Sel. Topics Appl. Earth Observ. Remote Sens.*, vol. 11, no. 10, pp. 3434–3442, Oct. 2018, doi: 10.1109/jstars.2018.2835647.

[34] C. Gomez et al., "Canopy height estimation in Mediterranean forests of Spain with TanDEM-X data," *IEEE J. Sel. Topics Appl. Earth Observ. Remote Sens.*, vol. 14, pp. 2956–2970, Feb. 2021, doi: 10.1109/jstars.2021.3060691.

[35] M. Schlund, A. Wenzel, N. Camarretta, C. Stiegler, and S. Erasmi, "Vegetation canopy height estimation in dynamic tropical landscapes with TanDEM-X supported by GEDI data," *Methods Ecol. Evol.*, vol. 14, no. 7, pp. 1639–1656, 2022, doi: 10.1111/2041-210x.13933.

[36] R. Touzi, A. Lopes, J. Bruniquel, and P. W. Vachon, "Coherence estimation for SAR imagery," *IEEE Trans. Geosci. Remote Sens.*, vol. 37, no. 1, pp. 135–149, Jan. 1999.

[37] C. Zeng, H. Shen, and L. Zhang, "Recovering missing pixels for Landsat ETM+ SLC-off imagery using multi-temporal regression analysis and a regularization method," *Remote Sens. Environ.*, vol. 131, pp. 182–194, 2013, doi: 10.1016/j.rse.2012.12.012.

[38] Y. Ke, J. Im, J. Lee, H. Gong, and Y. Ryu, "Characteristics of Landsat 8 OLI-derived NDVI by comparison with multiple satellite sensors and in-situ observations," *Remote Sens. Environ.*, vol. 164, pp. 298–313, 2015.

[39] R. Vallejo-Bombín, "The Spanish forest map scale 1: 50000 (MFE50) as base for the third national forest inventory," *Cuadernos de la Sociedad Española de Ciencias Forestales*, vol. 19, pp. 205–210, 2005.

[40] H. Lu, Z. Suo, R. Guo, and Z. Bao, "S-RVoG model for forest parameters inversion over underlying topography," *Electron. Lett.*, vol. 49, no. 9, pp. 618–620, 2013, doi: 10.1049/el.2012.4467.

[41] H. Chen, S. R. Cloude, D. G. Goodenough, D. A. Hill, and A. Nesdoly, "Radar forest height estimation in mountainous terrain using TanDEM-X coherence data," *IEEE J. Sel. Topics Appl. Earth Observ. Remote Sens.*, vol. 11, no. 10, pp. 3443–3452, Oct. 2018, doi: 10.1109/jstars.2018.2866059.
[42] C. Choi et al., "Large-scale forest height mapping by combining TanDEM-X and GEDI data," *IEEE J. Sel. Topics Appl. Earth Observ. Remote Sens.*, vol. 16, pp. 2374–2385, Feb. 2023.
[43] C. Wang, L. Wang, H. Fu, Q. Xie, and J. Zhu, "The impact of forest density on forest height inversion modeling from polarimetric InSAR data," *Remote Sens.*, vol. 8, no. 4, 2016, Art. no. 291.
[44] M. Pourshamsi, M. Garcia, M. Lavalle, and H. Balzter, "A machine-learning approach to PolInSAR and LiDAR data fusion for improved tropical forest canopy height estimation using NASA AfriSAR campaign data," *IEEE J. Sel. Topics Appl. Earth Observ. Remote Sens.*, vol. 11, no. 10, pp. 3453–3463, Oct. 2018, doi: 10.1109/jstars.2018.2868119.
[45] Y. Xie, H. Fu, J. Zhu, C. Wang, and Q. Xie, "A LiDAR-aided multi-baseline PolInSAR method for forest height estimation: With emphasis on dual-baseline selection," *IEEE Geosci. Remote Sens. Lett.*, vol. 17, no. 10, pp. 1807–1811, Oct. 2020, doi: 10.1109/lgrs.2019.2951805.
[46] M. Pourshamsi et al., "Tropical forest canopy height estimation from combined polarimetric SAR and LiDAR using machine-learning," *ISPRS J. Photogramm. Remote Sens.*, vol. 172, pp. 79–94, 2021, doi: 10.1016/j.isprsjprs.2020.11.008.
[47] X. X. Zhu et al., "Deep learning meets SAR: Concepts, models, pitfalls, and perspectives," *IEEE Geosci. Remote Sens. Mag.*, vol. 9, no. 4, pp. 143–172, Dec. 2021, doi: 10.1109/mgrs.2020.3046356.
[48] X. Sun, B. Wang, M. Xiang, L. Zhou, S. Wang, and S. Jiang, "Machine-learning inversion of forest vertical structure based on 2-D-SGVBVoG model for P-band Pol-InSAR," *IEEE Trans. Geosci. Remote Sens.*, vol. 60, Apr. 2022, Art. no. 5225115, doi: 10.1109/TGRS.2021.3091541.

Tao Zhang received the bachelor's and master's degrees in geodesy and survey engineering, in 2019 and 2022, respectively, from the School of Geosciences and Info-Physics, Central South University, Changsha, China, where he is currently working toward the Ph.D. degree in photogrammetry and remote sensing.

His research interests include polarimetric SAR and interferometric SAR data processing and its applications in the estimation of forest parameters.

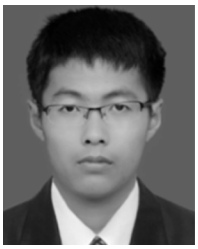

Haiqiang Fu (Senior Member, IEEE) received the bachelor's degree in remote sensing science and technology from Southwest Jiaotong University, Chengdu, China, in 2011, and the master's and Ph.D. degrees in geodesy and survey engineering from Central South University, Changsha, China, in 2014 and 2018, respectively.

He is currently an Associate Professor with the School of Geosciences and Info-Physics, Central South University. His research interests include polarimetric SAR interferometry and its applications for monitoring forest parameters and extracting the underlying topography over forest areas.

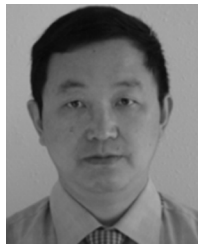

Jianjun Zhu received the M.Eng. degree in engineering surveying and the Ph.D. degree in geodesy and surveying engineering from the Central South University of Technology (now Central South University), Changsha, China, in 1985 and 1998, respectively.

From 1998 to 1999, he was a Research Assistant with the Department of Land Surveying and Geo-informatics, The Hong Kong Polytechnic University, Hong Kong. From 2000 to 2001, he was a Postdoctoral Fellow with the Center for Research on Geomatics, Laval University, Québec City, Canada. He is currently a Full Professor with the School of Geosciences and Info-Physics, Central South University. His research interests include the theory of errors and surveying adjustment and its applications in interferometric satellite synthetic aperture radar.

Juan M. Lopez-Sanchez (Senior Member, IEEE) received the Ingeniero (M.S.) and Doctor Ingeniero (Ph.D.) degrees in telecommunication engineering from the Technical University of Valencia, Valencia, Spain, in 1996 and 2000, respectively.

From 1998 to 1999, he was a Predoctoral Grantholder with Space Applications Institute, Joint Research Centre of the European Commission, Ispra, Italy. Since 2000, he has been leading the Signals, Systems and Telecommunication Group with the University of Alicante, Alicante, Spain, where he has been a Full Professor since November 2011. His research interests include microwave remote sensing for inversion of biophysical parameters, polarimetric and interferometric techniques, SAR imaging algorithms, and applications of radar remote sensing in agriculture and geophysics.

Dr. Lopez-Sanchez was the recipient of the Indra Award for the Best Ph.D. Thesis about radar in Spain in 2001. From 2006 to 2012, he was the Chair of the Spanish Chapter of the IEEE Geoscience and Remote Sensing Society. He has coauthored more than 100 papers in refereed journals and more than 150 papers and presentations at international conferences and symposia.

Cristina Gómez received the M.Sc. degree in applied geospatial technologies from the University of Aberdeen, Aberdeen, U.K., in 2006, and the Ph.D. degree in conservation and sustainable use of forest systems from the University of Valladolid, Valladolid, Spain, in 2014.

She was an M.Sc. Forest Engineer with the Technical University of Madrid, Madrid, Spain, in 2001. Her current research focuses on the characterization and monitoring of environmental dynamics at different spatiotemporal scales, integrating a range of geospatial technologies. She employs time-series analysis of remotely sensed data for assessment of forest processes of change, such as drastic and subtle disturbance, or natural succession, including regeneration, growth, decline, and mortality. She is particularly interested in forest phenological traits and variations through time, as well as long-term trends of change to help assessing forest structure and ecosystemic services.

Changcheng Wang (Member, IEEE) received the Ph.D. degree in photogrammetric and remote sensing from the State Key Laboratory of Information Engineering in Surveying, Mapping and Remote Sensing, Wuhan University, Wuhan, China, in 2008.

From 2009 to 2011, he was a Lecturer with Central South University, Changsha, China, where he has been a Professor with the School of Geosciences and Info-Physics since 2011. His research interests include synthetic aperture radar (SAR), Interferometric SAR (InSAR), and polarimetric InSAR methods and applications for geosciences.

Wenjie He received the bachelor's and master's degrees in geodesy and survey engineering, in 2015 and 2018, respectively, from Central South University, Changsha, China, where he is currently working toward the Ph.D. degree in geodesy and surveying engineering.

His research interests include PolSAR interferometry and its applications for monitoring forest parameters over forest areas.

Zhiwei Liu received the master's degree in geodesy and survey engineering in 2019 from Central South University, Changsha, China, where he is currently working toward the Ph.D. degree in geodesy and surveying engineering.

His research interests include InSAR data processing and its applications. He is currently a joint Ph.D. student with the University of Alicante, Alicante, Spain.